Electronic Supplementary Information

Large-area Transparent Flexible Guanidinium Incorporated $MAPbI_3$ Microstructures for High-performance Photodetectors with Enhanced Stability

Gundam Sandeep Kumar,[a] Piyush Kanti Sarkar,[a] Bapi Pradhan,[a] Mozakkar Hossain,[a,b] K. D. M. Rao,[a,b]* and Somobrata Acharya[a]*

[a] School of Applied & Interdisciplinary Sciences, Indian Association for the Cultivation of Science, Jadavpur, Kolkata-700032, India.

Email: camsa2@iacs.res.in

[b] Technical Research Centre, Indian Association for the Cultivation of Science, Jadavpur, Kolkata-700032, India.

Email: trckdmr@iacs.res.in

Table of Content

1. Experimental Methods:

Materials. Hydroiodic acid (HI, 48% in water), methylamine solution (40% in methanol) were purchased from Merck chemicals, and Guanidinium Iodide (GuaI), Lead Iodide (PbI_2) were purchased from the Sigma-Aldrich and used without further purification.

Preparation of Perovskite Precursor Solutions. Methylammonium iodide (MAI) was synthesized using a reported protocol from literature.[1] In brief, a 50 mL hydroiodic acid (48% in water) is added dropwise to 30 mL of methylamine solution (40% in methanol) in a round bottom flask at 0 °C while continuous stirring for 2 h. After the precipitation formation, the solvent in the reaction solution is removed by rotary evaporation at 50 °C for 1 h. Purification of the products is conducted by dissolving in ethanol, recrystallizing from diethylether, and drying at room temperature in a vacuum oven for 24 h. The washing and recrystallization process were repetitively done to obtain high-purity MAI crystals. Finally, the $MAPbI_3$ precursor solutions (10 wt.%) were prepared by dissolving the MAI and PbI_2 (Sigma Aldrich) with 1:0.8 molar ratio in 1 ml of anhydrous N, N-dimethylformamide (DMF) at 60 °C and performing continuous stirring for 12 h. For the preparation of the Gua cation mixed $MAPbI_3$ perovskite precursor solution, stoichiometric precursor solutions were prepared by mixing GuaI, MAI, and PbI_2 in a mixed solution of DMF and N, N′ -dimethylsulfoxide (DMSO) (9:1 volume ratio) with GuaI/MAI of ~ 0.12:0.88 and ~ 0.33:0.67 molar ratio, while keeping the PbI_2 molarity equal to 0.8.

Spray Coating Process of RPMs and device fabrication. For the preparation of RPMs, we have used the pressure-controlled spray coating technique. We have used a spray gun with a nozzle diameter of ~ 0.3 mm and the corresponding flow rate is ~ 0.05 cm^3/sec. Initially, the perovskite precursor solution with a concentration of 10 wt.% (100 mg/ml) is loaded into filler of the spray gun. The PET/glass substrates were placed on a hot plate at distance of 18 cm and a constant temperature of ~ 110 °C is maintained prior to the spray coating. The surface texture of PET was checked by optical microscope to confirm that heating at 110 °C does create any deformation. The precursor solution is spray coated on PET/glass substrates for 4 seconds with a nitrogen gas pressure of ~ 15 psi and continued to annealing at the substrates at same temperature for 2 min. After the spray coating process on the substrate, yellow precursor was instantaneously turned into brown in color to form perovskite phase. The total spray coating process was carried out in ambient conditions where the humidity levels ~ 45-55%.

RPMs based photodetectors were fabricated on commercially available Au electrodes on top of Silicon Oxide /Silicon substrates with a channel width of ~ 100 nm and 50 μm (QUDOS Technology LTD). For the flexibility test, vacuum deposited Ag electrodes with a channel width of ~ 100 μm channel length and 2 mm PET substrates were used. RPMs were spray coated on PET substrate with pre-fabricated Ag electrodes. The resulting substrates were mounted on a teflon mold to bend the devices with specific bending angles such as 20°, 30°, 45°, and 60°.

Materials Characterization. The $MA_{1-x}Gua_xPbI_3$ RPMs with different molar ratio of mixed cations of were characterized in solid state conditions. SEM imaging on RPMs was performed using the ZEISS (ZEISS EVO-MA 10). X-Ray diffraction measurements were carried out by using Bruker AXS D8 Advanced equipment (40 kV, 40 mA, wavelength ~ 0.15406 nm) with Cu Kα radiation. UV-vis absorbance/transmittance measurements were performed by using Varian Cary 5000 UV-vis-NIR spectrophotometer.

Characterization of the Photodetectors. The current–voltage characteristic measurements were carried out with the help of semiconductor characterization system (Keithley 4200 SCS) and TTPx Lakeshore probe-station. For photoconductivity measurements, Newport Solar Simulator (model:66902) of 1 sun AM1.5G (~100 mW/cm^2) light source and Optem Schott white light source with variable power intensities were used. The optical power density was measured by using the power meter (CHY 332 lightmeter). The wavelength dependent photocurrent measurements were performed using Newport Solar Simulator connected with monochromator (Model 74125). The transient photocurrent measurements were conducted with a red LASER diode (LD-RL-6-5v, ~ 3 mW, 650 nm), optical chopper (Thorlabs - MC2000B-EC), Lakeshore probe-station and oscilloscope (Scientific Instruments). All the photoresponse measurements and stability were performed in ambient conditions with humidity ~ 45-55%.

2. Microscopic images of random percolative microstructures (RPMs):

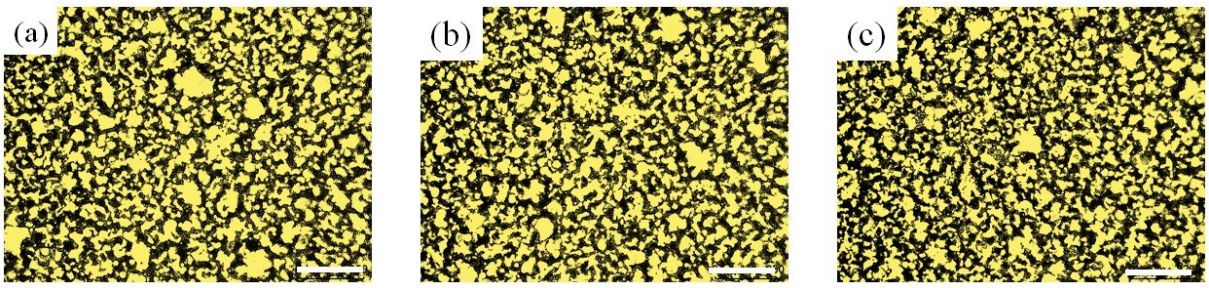

Fig. S1 (a-c) Microscopic images of $MA_{0.88}Gua_{0.12}PbI_3$ perovskite RPMs. Scale bar is 250 μm.

3. Microscopic images of various composition perovskite RPMs:

The optical microscope imaging was conducted and reveals the excellent interconnectivity of the RPMs from one end to the other end over a large substrate area.

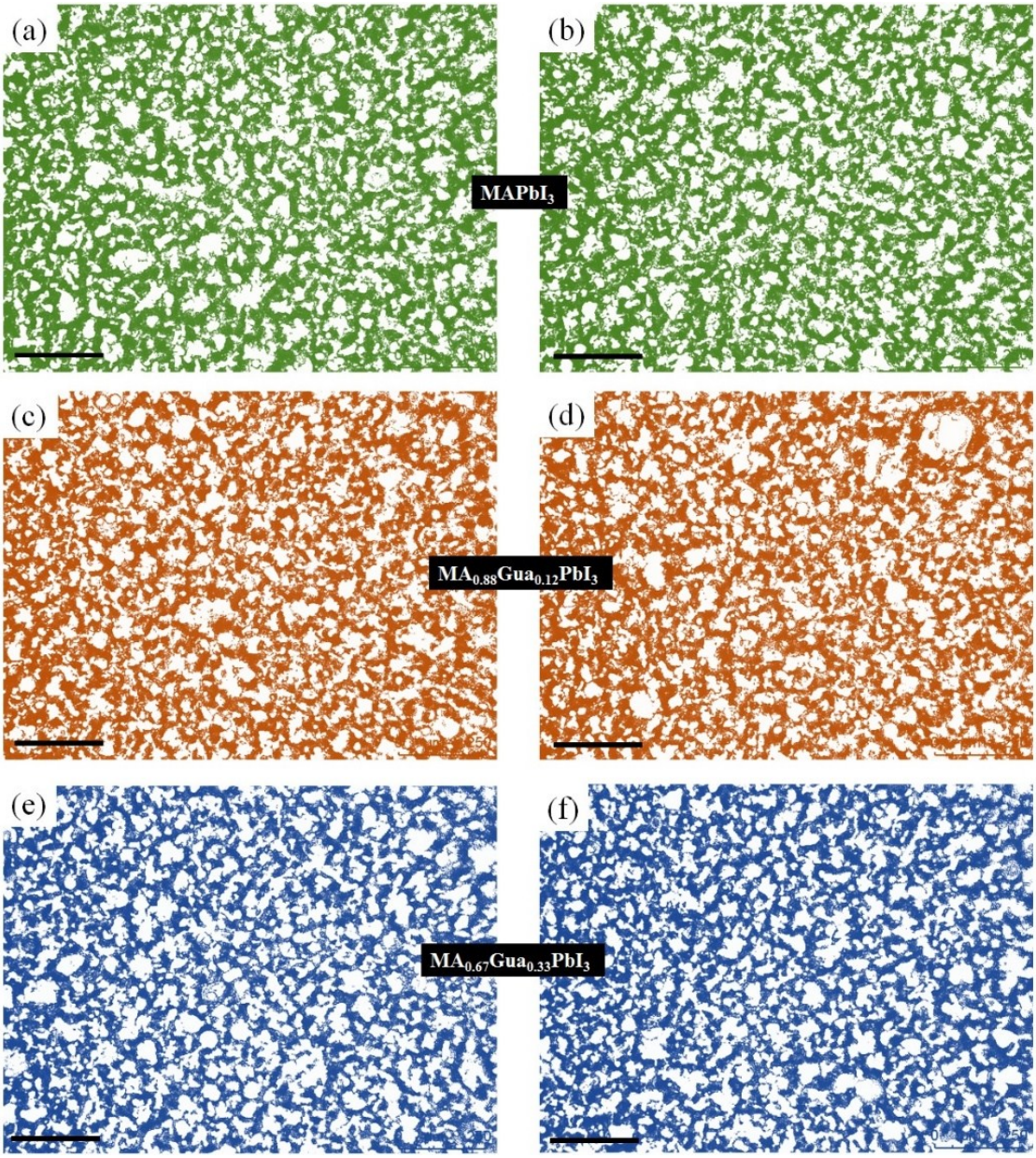

Fig. S2 Optical microscopic images of RPMs; (a, b) $MAPbI_3$, (c, d) $MA_{0.88}Gua_{0.12}PbI_3$, and (e, f) $MA_{0.67}Gua_{0.33}PbI_3$. (Scale bar 250 μm)

4. SEM images of RPMs:

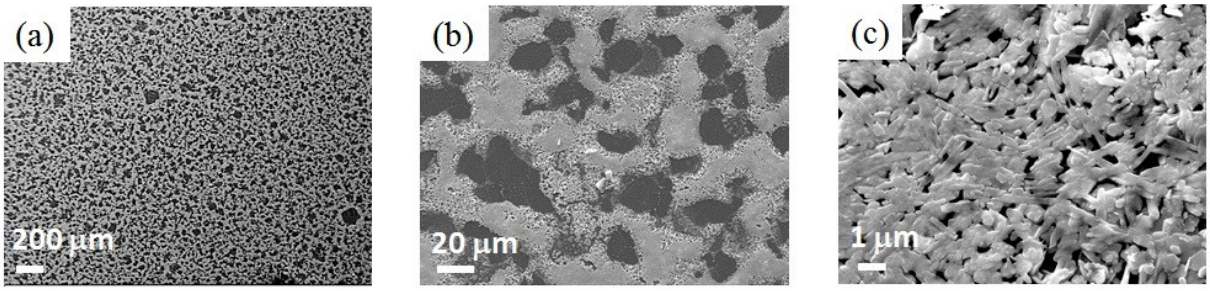

Fig. S3 (a-c) SEM images of $MA_{0.67}Gua_{0.33}PbI_3$ RPMs at different magnifications. (x=0.33)

5. XRD diffraction pattern comparison:

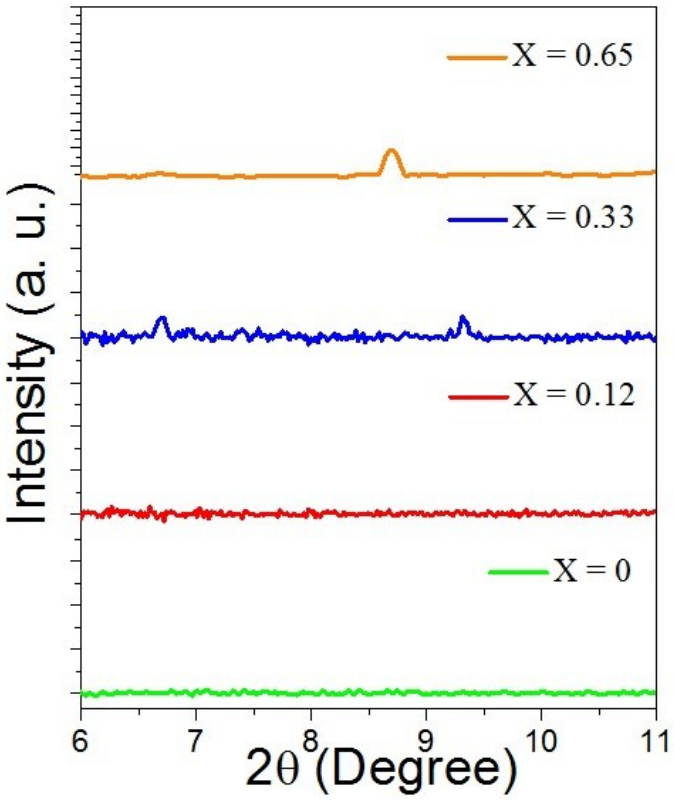

Fig. S4 XRD diffraction pattern comparison. XRD pattern of $MA_{0.67}Gua_{0.33}PbI_3$ and $MA_{0.35}Gua_{0.35}PbI_3$ perovskites introduces additional peaks at lower diffraction angles compared to the $MAPbI_3$ and $MA_{0.88}Gua_{0.12}PbI_3$, confirms the formation of 1D-$GuaPbI_3$ perovskites. Higher content (33%) of Gua cation leads to formation of phase-segregated 1D-$GuaPbI_3$ and consistent with the observed SEM morphology.

6. Microscopic image and fill factor:

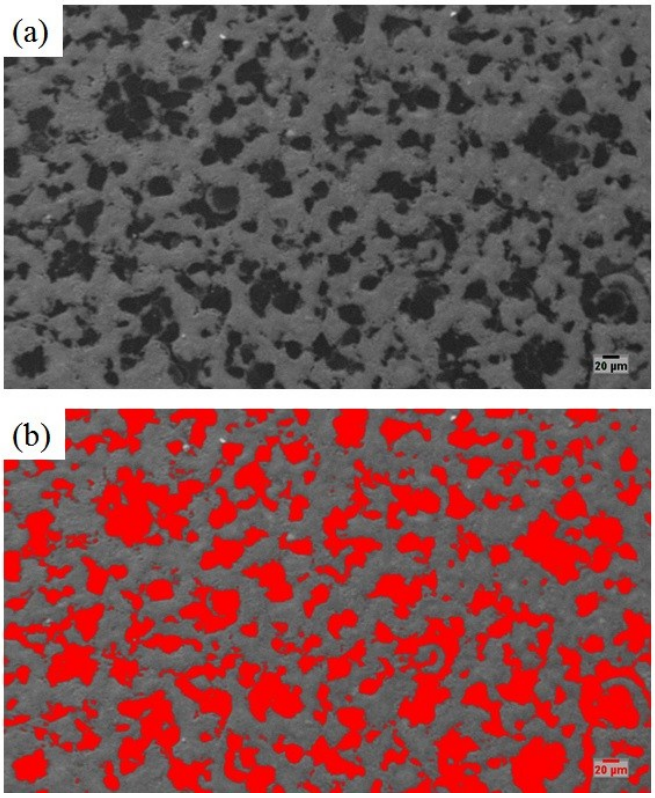

Fig. S5 (a) SEM Image, and (b) calculating the fill factor of RPMs from image J software.

7. UV-vis and Transmittance spectra of $MA_{0.67}Gua_{0.33}PbI_3$:

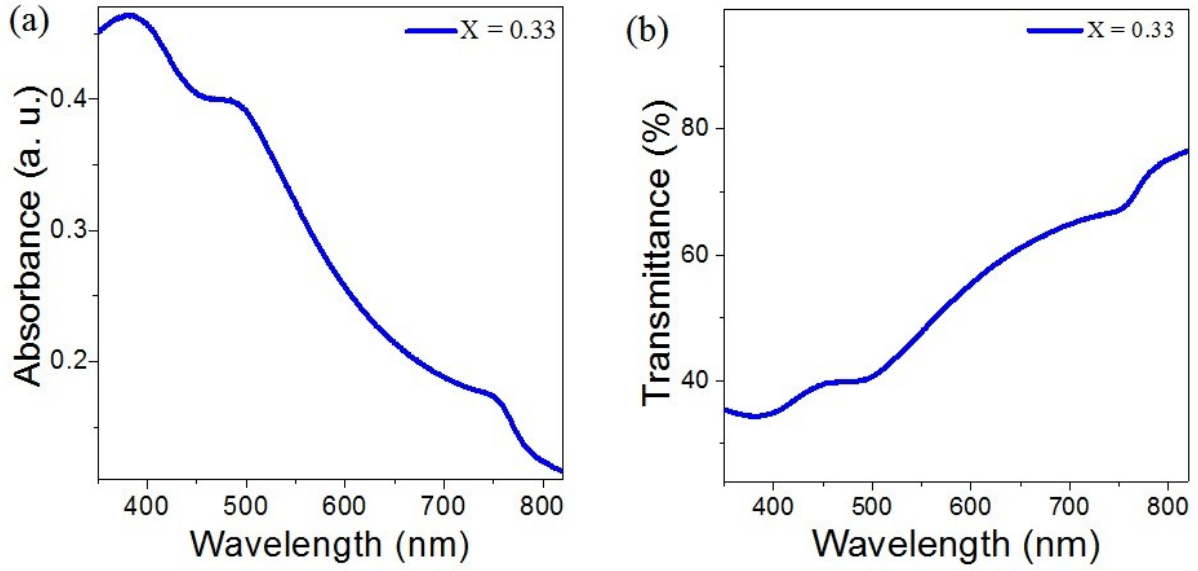

Fig. S6 (a) UV-vis, and (b) Transmittance spectra of $MA_{0.67}Gua_{0.33}PbI_3$ RPMs.

8. Photodetector Figure of Merits (FOMs) and comparison of devices:

The working principle of photodetector can be expressed as, when the device illuminated by light, the electron−hole pairs were generated by following the photoelectric effect. Then the generated electron−hole pairs were separated and collected by electrodes under the external applied electric field.

Here, we measured all the FOM of the perovskite photodetectors, such as Responsivity (R), Detectivity (D), and External quantum efficiency (EQE).[2,3]

The responsivity of the photodetector calculated as follows:

$$R = \frac{I_{ph}}{P_0 \cdot S} \quad \text{..... (S1)}$$

Where;

$I_{ph} = I_p - I_d$, is the difference between the photocurrent and dark current

P_0= The illuminated light power density

S = Effective area of the photodetector.

Besides, we evaluated the specific detectivity (D*) and the EQE of the photodetector according to the following relations:

$$D^* = \frac{R_\lambda A^{1/2}}{(2eI_d)^{1/2}} \quad \text{..... (S2)}$$

$$EQE = R_\lambda \frac{hc}{e\lambda} \quad \text{..... (S3)}$$

Where;

R_λ = Responsivity of the photodetector measured at a specific monochromatic wavelength

A or S = Active area of the photodetector

e = Elementary charge

I_d = Dark current of the photodetector

h = Planck's constant

c = Velocity of light

λ = Wavelength of the monochromatic light

"Figure of Merits" comparison of RPMs:

Responsivity, Detectivity, and EQE comparison of $MAPbI_3$, $MA_{0.88}Gua_{0.12}PbI_3$, and $MA_{0.67}Gua_{0.33}PbI_3$ RPMs.

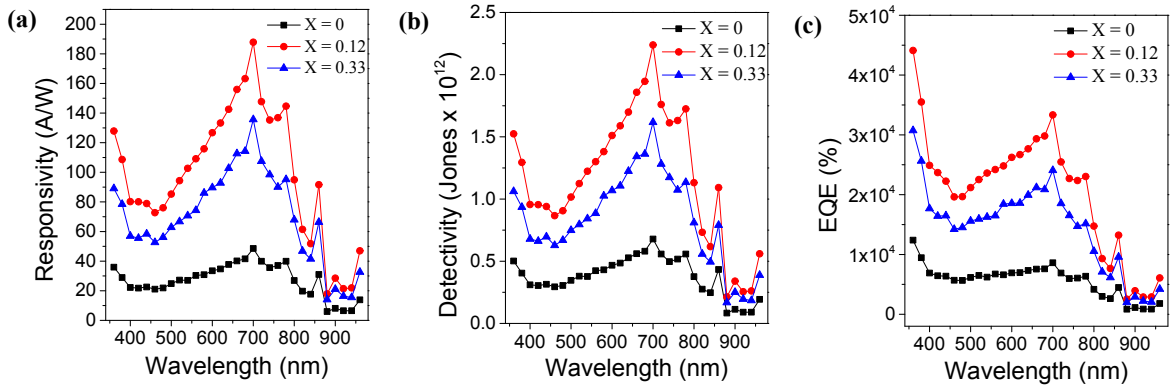

Fig. S7 Comparison of Figure of merits of $MAPbI_3$, $MA_{0.88}Gua_{0.12}PbI_3$, and $MA_{0.67}Gua_{0.33}PbI_3$ RPMs; (a) Responsivity, (b) Detectivity, and (c) EQE.

9. Table S1: Comparison of some of Figure of merits of mixed cation perovskite-based photodetectors.

Reference	Photo-active material	Applied Bias (V)	R (A/W)	D (Jones)	EQE (%)	Response time	Flexibility and Cycles
4	$FA_xMA_{(1-x)}PbI_3$	10	10.57	--	--	9.0 ms	No
5	$MA_{0.45}FA_{0.55}PbI_3$	-4	--	--	40	200 µs	No
6	$MA_{0.5}FA_{0.5}Pb_{0.5}Sn_{0.5}I_3$	----	0.2	10^{12}	--	7.4 µs	No
7	Cs/FA/$MAPbI_3$	10	1.63	$>10^{13}$	317	19µs	No
8	$MA_{0.975}Rb_{0.025}Sn_{0.65}Pb_{0.35}I_3$	----	0.4	10^{12}	0.5	40 ns	No
9	$(C_4H_9NH_3)_2(CH_3NH_3)_2Pb_3Br_{10}$	5	--	3.6 x 10^{10}	60	150µs	No
10	$(iBA)_2(MA)_{n-1}Pb_nI_{3n+1}$	1.5	0.11	--	--	16 ms	No

11	$FA_{0.85}Cs_{0.15}PbI_3$	0	5.7	2.7 x 10^{13}		45 ns	No
12	$Cs_x(CH_3NH_3)_{1-x}PbI_3$	5	23	2.5 x 10^{11}	5400	--	No
13	$(RNH_3)_2(CH_3NH_3)_{n-1}M_nX_{3n+1}$	30	0.012	--	--	10 ms	No
14	$(OA)_2FA_{n-1}Pb_nBr_{3n+1}$	9	32	--	7100	0.25 ms	No
15	$FA_{(1-x)}MA_xPbI_3$	2	0.064	--	--	--	No
16	$FA_{0.83}Cs_{0.17}Pb[I_{0.9}Br_{0.1}]_3$	-2	33	10^{11}	7960	260 ns	Yes
17	$FA_{0.7}Rb_{0.3}PbI_3$	0	0.43	1.7 × 10^{12}	40–70	300 ns	No
18	$FA_{0.7}Cs_{0.3}Pb(I_{0.8}Br_{0.2})_3$	0.8	5.0	3.62 × 10^{13}	--	108 μs	Yes, 10000
19	Cesium-doped triple cation perovskites	10	1.62	7.7 × 10^{12}	512	38.6 ms	Yes, 2000
This work	**$MA_{0.88}Gua_{0.12}PbI_3$**	**0.9**	**187**	**2.23 x 10^{12}**	**44115**	**390** μs	**Yes, 1000**

10. Table S2: Comparison of Figure of merits of transparent perovskite-based photodetectors with $MA_{0.88}Gua_{0.12}PbI_3$.

Reference	**Photo-active material**	**Applied Bias (V)**	**R (A/W)**	**D (Jones)**	**EQE (%)**	**Response time**	**Flexibility and Cycles**	***T**
20	$CH_3NH_3PbI_3$	10	0.10	1.02 x 10^{12}	--	0.3 ms	Yes, 10000	50 %
21	$CH_3NH_3PbI_3$	26	4.29 x 10^{-3}	--	--	50μs	No	60 %
22	$(C_4H_9NH_3)_2PbBr_4$	0.5	32 x 10^{-3}	8.5 ×10^8	--	2 ms	No	75 %
23	$CsPbCl_3$	---	1.89	--	--	41 ms	No	90 %

24	$(C_4H_9NH_3)_2PbBr_4$	0.6	0.55	2.16 x 10^{10}	--	10 ms	No	60%
25	TiO_2 NTs/$MAPbI_3$ QDs	1	1.3	2.5 x 10^{12}	--	2 s	Yes, 200	85%
This work	**$MA_{0.88}Gua_{0.12}PbI_3$**	**0.9**	**187**	**2.23 x 10^{12}**	**44115**	**390 µs**	**Yes, 1000**	50 %

*T=Transparency

11. Photoswitching behaviour:

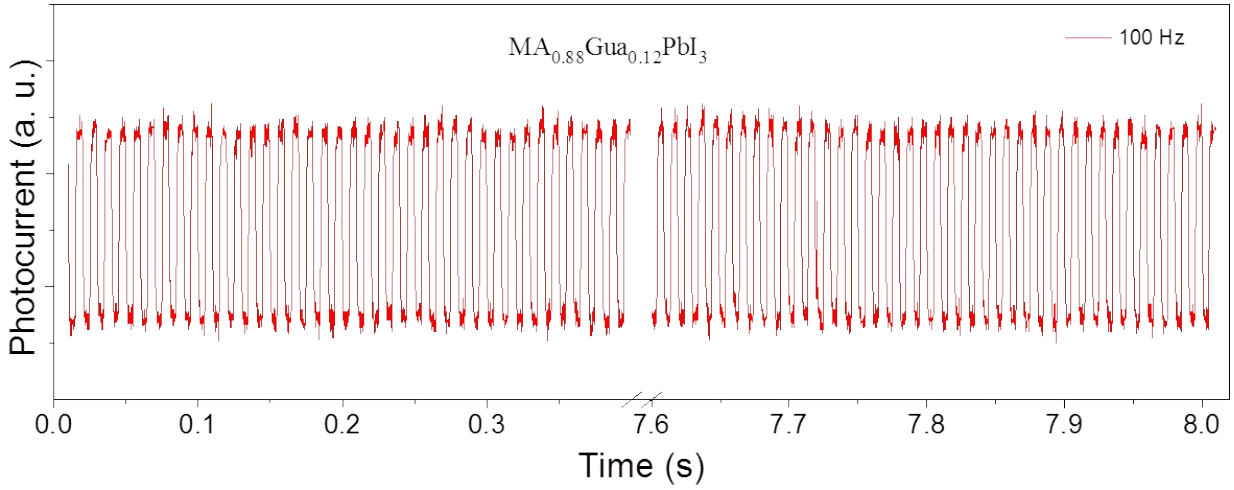

Fig. S8 Photoswitching repeatability test of $MA_{0.88}Gua_{0.12}PbI_3$, over 800 cycles at 100 Hz.

12. Exponential fitting to estimate the response time of the photodetector:

Rise time equation; $I = I_0 - I_0 \times e^{(-\frac{x}{t_r})}$ ……. (S4)

Fall time equation; $I = I_0 + A_1 \times e^{(-\frac{x}{t_f})}$ ……..…….. (S5)

Where;

I = Current,

I_0 = Initial value of current,

A_1 = Independent variable,

t_r = Rise time,

t_f = Fall time,

x = Time

The significant saturation of both the dark and light currents were observed at modulated frequencies of up to 100 Hz, and 800 cycles representing the saturated ON (under light) and OFF (in dark) state at 100 Hz is shown in Fig. S8.

13. Microscopic image of Ag electrodes:

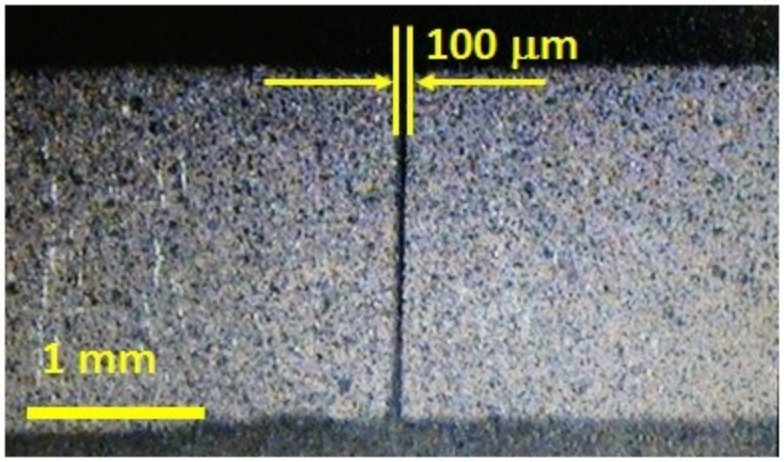

Fig. S9 Perovskite RPMs on flexible PET substrates with Ag electrodes.

14. Figure of merits of the photodetector devices fabricated on PET substrate with 100 µm channel length:

We have measured the photodetector performance parameters for the device fabricated on flexible PET substrates with electrode gap of 100 µm. A maximum responsivity of ~ 275 mA/W, detectivity of ~ 2.43 x 10^{11} jones and EQE of ~68.2% were obtained. These values are less compared to the devices fabricated on SiO_2/Si substrate with electrode gap of 100 nm. Such a decrease of the photodetector performance parameters is expected owing to the longer channel length.[26,27] Reducing the channel length is an effective approach to attaining the higher performance in the photodetector devices.[23]

15. Stability comparison of the photodetectors:

Aging the devices over 10 days, the photoresponse of the $MAPbI_3$ RPMs based photodetector device gradually decreased with the continuous illumination of light for more than 600 s, while the $MA_{0.88}Gua_{0.12}PbI_3$ RPMs based photodetector showed stable photoresponse under the continuous illumination of light.

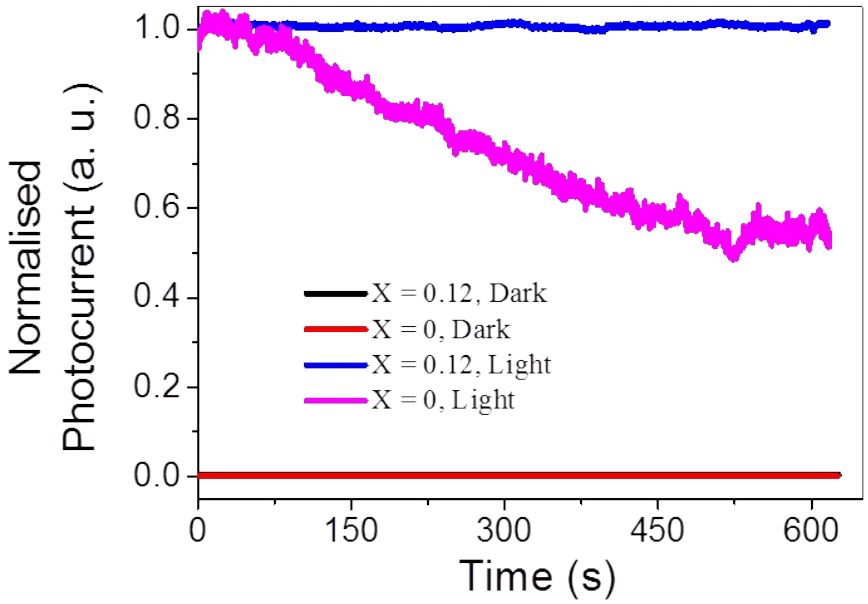

Fig. S10 Normalised photoresponse stability of $MAPbI_3$ and $MA_{0.88}Gua_{0.12}PbI_3$ after 10 days.

References

1. M. Saliba, J.-P. Correa-Baena, C. M. Wolff, M. Stolterfoht, N. Phung, S. Albrecht, D. Neher and A. Abate, *Chem. Mater.* 2018, **30**, 4193–4201.
2. Z. Lian, Q. Yan, Q. Lv, Y. Wang, L. Liu, L. Zhang, S. Pan, Q. Li, L. Wang and J.-L. Sun, *Sci. Rep.* 2015, **5**, 16563.
3. X. Cheng, L. Jing, Y. Zhao, S. Du, J. Ding and T. Zhou, *J. Mater. Chem. C* 2018, **6**, 1579–1586.
4. S. Li, S. Tong, J.-Q. Meng, C. Zhang, C. Zhang, J. Shen, S. Xiao, J. Sun, J. He, Y. Gao, B. Yang and J. Yang, *Org. Electron.* 2018, **52**, 190–194.

5. W.-G. Li, H.-S. Rao, B.-X. Chen, X.-D. Wang and D.-B. Kuang, *J. Mater. Chem. A* 2017, **5**, 19431–19438.
6. X. Xu, C.-C. Chueh, P. Jing, Z. Yang, X. Shi, T. Zhao, L. Y. Lin and A. K.-Y. Jen, *Adv. Funct. Mater.* 2017, **27**, 1701053.
7. T. Zhang, J. Wu, P. Zhang, W. Ahmad, Y. Wang, M. Alqahtani, H. Chen, C. Gao, Z. D. Chen, Z. Wang and S. Li, *Adv. Opt. Mater.* 2018, **6**, 1701341.
8. H. L. Zhu, Z. Liang, Z.; Huo, W. K. Ng, J. Mao, K. S. Wong, W.-J. Yin and W. C. H. Choy, *Adv. Funct. Mater.* 2018, **28**, 1706068.
9. L. Li, Z. Sun, P. Wang, W. Hu, S. Wang, C. Ji, M. Hong and J. Luo, *Angew. Chem. Int. Ed.* 2017, **56**, 12150–12154.
10. R. Dong, C. Lan, X. Xu, X. Liang, X. Hu, D. Li, Z. Zhou, L. Shu, S. Yip, C. Li, S.-W. Tsang and J. C. Ho, *ACS Appl. Mater. Interfaces* 2018, **10**, 19019–19026.
11. F.-X. Liang, J.-Z. Wang, Z.-X. Zhang, Y.-Y. Wang, Y. Gao and L.-B. Luo, *Adv. Opt. Mater.* 2017, **5**, 1700654.
12. D. Dong, H. Deng, C. Hu, H. Song, K. Qiao, X. Yang, J. Zhang, F. Cai, J. Tang and H. Song, *Nanoscale* 2017, **9**, 1567–1574.
13. J. Zhou, Y. Chu and J. Huang, *ACS Appl. Mater. Interfaces* 2016, **8**, 25660–25666.
14. D. Yu, F. Cao, Y. Shen, X. Liu, Y. Zhu and H. Zeng, *J. Phys. Chem. Lett.* 2017, **8**, 2565–2572.
15. Y. Huang, L. Li, Z. Liu, H. Jiao, Y. He, X. Wang, R. Zhu, D. Wang, J. Sun, Q. Chen and H. Zhou, *J. Mater. Chem. A* 2017, **5**, 8537–8544.
16. D. G. Georgiadou, Y.-H. Lin, J. Lim, S. Ratnasingham, M. A. McLachlan, H. J. Snaith, and T. D. Anthopoulos, *Adv. Funct. Mater*. 2019, **29**, 1901371.
17. F. Yao P. Gui, C. Chen, B. Li, R. Li, C. Tao, Q. Lin and G. Fang, *ACS Appl. Mater. Interfaces* 2019, **11**, 39875−39881.

18. Y. Wang, X. Zhang, D. Wang, X. Li, J. Meng, J. You, Z. Yin and J. Wu, *ACS Appl. Mater. Interfaces* 2019, **11**, 28005−28012.

19. S. Tong, C. Gong, C. Zhang, G. Liu, D. Zhang, C. Zhou, J. Sun, S. Xiao, J. He, Y. Gao and J. Yang, *Applied Materials Today* 2019, **15**, 389–397.

20. H. Deng, X. Yang, D. Dong, B. Li, D. Yang, S. Yuan, K. Qiao, Y.-B. Cheng, J. Tang and H. Song, *Nano Lett.* 2015, **15**, 7963–7969.

21. Y. P. Jeon, S. J. Woo and T. W. Kim, *Appl. Surf. Sci.* 2018, **434**, 375–381.

22. M. Kumar, H.-S. Kim, D. Y. Park, M. S. Jeong and J. Kim, *Nanoscale* 2018, **10**, 11392–11396.

23. J. Zhang, Q. Wang, X. Zhang, J. Jiang, Z. Gao, Z. Jin and S. Liu (Frank), *RSC Adv.* 2017, **7**, 36722–36727.

24. M. Kumar, M. Patel, D. Y. Park, H.-S. Kim, M. S. Jeong and J. Kim, *Adv. Electron. Mater.* 2019, **5**, 1800662.

25. Z. Zheng, F. Zhuge, Y. Wang, J. Zhang, L. Gan, X. Zhou, H. Li and T. Zhai, *Adv. Funct. Mater.* 2017, **27**, 1703115.

26. Y. Peng, F. Guo, H. Xia, W. Lv, L. Sun, S. Xu, H. Zhu, X. Chen, C. Liu, Y. Wang and F. Lu, *Applied Optics* 2019, **58**, 1319-1326.

27. Y. Wang, Z. Xia, S. Du, F. Yuan, Z. Li, Z. Li, Q. Dai, H. Wang, S. Luo, S. Zhang and H. Zhou, *Nanotechnology* 2016, **27**, 175201.